

Liquids (Wiley, New York, 1964).

²²H. J. M. Hanley, R. D. McCarty, and J. V. Sengers, *J. Chem. Phys.* **50**, 857 (1969); also note the statement in this reference that the quadratic term does not contribute significantly till 200 amagat.

²³This kind of approach was noted in passing in Ref. 4 (for the potential expansion) and used in Ref. 9.

²⁴Similar formulas appear in R. Dashen and S.-K. Ma, *Phys. Rev. A* **4**, 700 (1971).

²⁵The effects of bound states are discussed in detail by K. Kawasaki and I. Oppenheim [*Phys. Rev.* **139**, A649 (1965)].

²⁶S. Chapman and T. G. Cowling, *The Mathematical Theory of Non-Uniform Gases*, 3rd ed. (Cambridge U. P., London, 1970).

²⁷J. Groeneveld, *Phys. Lett.* **3**, 50 (1962).

²⁸An expression for σ in terms of projection operators and the expansion to lowest order in the potential are given by A. Z. Akcasu, N. Corngold, and J. J. Duderstadt [*Phys. Fluids* **13**, 2213 (1970)].

²⁹A. R. Altenberger and J. Stecki, *J. Stat. Phys.* **5**, 83

(1972).

³⁰G. E. Uhlenbeck and G. W. Ford, *Lectures in Statistical Mechanics* (American Mathematical Society, Providence, R.I., 1963).

³¹Reference 19, Eqs. (3.44) and (3.47).

³²J. V. Sengers, *Phys. Fluids* **9**, 1333 (1966); J. V. Sengers, M. H. Ernst, and D. T. Gillespie, *J. Chem. Phys.* **56**, 5583 (1972).

³³See S. K. Kim and J. Ross, *J. Chem. Phys.* **42**, 263 (1965), and the relevant references therein.

³⁴The insensitivity of $S(k\omega)$ to the details of the repulsive potential at low densities was noted by A. Sugawara, S. Yip, and L. Sirovich [*Phys. Fluids* **11**, 925 (1968)]. Also, the comparison of these calculations (based on repulsive potentials) with experiments on gaseous xenon shows good agreement, indicating that the effect of the attractive part of the potential on $S(k\omega)$ would not be great. For this comparison and a general review see S. Yip, *J. Acoust. Soc. Am.* **49**, 941 (1971).

Nuclear Magnetic Susceptibility of Solid He³ and of Dilute Solid Mixtures of He⁴ in He³†

T. P. Bernat* and H. D. Cohen‡

Physics Department, Brandeis University, Waltham, Massachusetts 02154

(Received 11 December 1972)

Continuous-wave NMR was used to study the temperature dependence of the static nuclear magnetic susceptibility of solid He³ and solid mixtures of He⁴ in He³. Measurements were performed in the purest sample (3.7×10^{-5} He⁴ in He³) at four molar volumes (21, 22, 23, and 24 cm³/mole) in the bcc phase, and at several He⁴ concentrations ranging from 3.7×10^{-5} to 2.0×10^{-2} at 21 and 23 cm³/mole. The temperature range of the measurements was from 0.95 to 0.32 K. The data were fitted to a Curie-Weiss law with an rms deviation from best fit of less than 10^{-3} and best values of the Weiss constant θ were obtained. Susceptibilities and temperatures were measured to better than 0.1%. The temperature scale was based upon the susceptibility of the purest, most-dense sample. The desired accuracy in the susceptibility measurements necessitated a new method of data reduction. The accuracy in the extracted values of θ was better than ± 1 mk. The values of θ in the purest sample (-0.24 ± 0.82 mK at 21 cm³/mole, -1.03 ± 1.06 mK at 22 cm³/mole, -1.49 ± 0.27 mK at 23 cm³/mole, and -3.07 ± 0.78 mK at 24 cm³/mole) agreed within experimental uncertainty with those of earlier workers, operating at lower temperatures. They provide a high-temperature check on those measurements. The measured effects on θ of the He⁴ impurity are consistent with the work of Richards and Homer, but the measurements show an improved accuracy. The data, as a function of x , the atomic fraction of He⁴, have been fitted to the equation $\theta(x) = \theta_0(1 + Kx)$. Values of K of -430 ± 450 and -19 ± 10 were obtained at 21 and 23 cm³/mole, respectively.

I. INTRODUCTION

During the past decade there has been considerable theoretical¹⁻²⁰ and experimental²¹⁻⁴⁸ interest in those properties of pure solid He³, as well as solid mixtures of He⁴ and He³, which depend upon the exchange interaction between He³ nuclei. Many of these properties have been described by means of a Heisenberg Hamiltonian

$$H_x^{3,3} = -2J \sum_{\langle mn \rangle} \vec{S}_i \cdot \vec{S}_j \quad (1)$$

together with the usual dipole-dipole and Zeeman terms, where J is the exchange energy and the no-

tation ($\langle mn \rangle$) indicates a sum over nearest-neighbor pairs only.⁴⁹ In the presence of He⁴ impurities, a second term^{15,18} has been added to Eq. (1) in order to describe the exchange between a He³ and a He⁴ atom;

$$H_x^{3,4} = -2J'' \sum_{\langle mn \rangle, \sigma} D_{i\sigma}^+ D_{j\sigma}^- \quad (2)$$

where we have used a notation similar to that of Balakrishnan and Lange.¹⁸ It is possible that the presence of He⁴ in the He³ lattice also leads to modification of Eq. (1) by creating a local distortion around the He⁴ atom.¹³ This distortion might produce an enhanced value of J .

In solid helium the combined effects of small atomic mass and weak interatomic potential produce a large spread in single-particle wave functions around the equilibrium lattice sites, with an accompanying large zero-point motion and near-neighbor wave function overlap. The probability of exchange between neighboring helium atoms is thus relatively large, and this is reflected in non-negligible values of nuclear exchange interaction, a situation unique to solid He^3 . Further, the magnitudes of J and J'' can be varied over a wide range in solid helium by changing the interatomic distance through pressurization.

Experimental investigation of those properties of pure⁵⁰ solid He^3 influenced by Eq. (1) allow measurement of J . In particular, at temperatures less than a few tenths of a degree below the melting point, $\text{H}_x^{3,3}$ plays a major role in determining the modulation of the dipolar fields at individual nuclei, and thus the nonequilibrium dynamics of the spin system. Magnitudes for the exchange energy J can be deduced from measurements of the transverse and longitudinal nuclear relaxation times. Relevant experiments^{23,24,26-29} and their interpretations have been reviewed by Guyer, Richardson, and Zane,⁵¹ as well as by Richards.⁵² $\text{H}_x^{3,3}$ also strongly influences the equilibrium thermodynamics of the solid below about 0.2 K, which provides the basis for the extraction of exchange energies from the pressure-vs-temperature measurements performed by Adams and co-workers³¹ in Florida. In addition, $\text{H}_x^{3,3}$ strongly affects the melting curve of He^3 below about 10 mK, as seen in the experiments of Wheatly and co-workers.³⁵

Finally, $\text{H}_x^{3,3}$ influences the equilibrium magnetic properties of the solid and predicts a nuclear alignment temperature in low magnetic fields of order $|J|/k$. Sufficiently far above this temperature the nuclear magnetic susceptibility closely follows a Curie-Weiss law,

$$\chi = \frac{C}{T - \theta} \quad (3)$$

with a Weiss constant for a bcc lattice given by

$$\theta = 4J/k \quad (4)$$

(see Ref. 53).

Early susceptibility measurements in pure^{21,22,25,32} He^3 were not accurate enough to unambiguously determine J , but at best could put upper bounds on $|J|$. The more recent and more accurate work of several groups^{37-39,42} has, however, shown that θ , as defined in Eq. (3), and thus J , is negative in the bcc phase, implying antiferromagnetic ordering at very low temperatures. Additional evidence⁴⁸ is provided by measurements of P vs T in the presence of high magnetic fields, though a very similar experiment did not obtain this result.⁴⁷

Determinations of J in pure He^3 by the methods just described have been thoroughly reviewed in a paper by Richardson.⁵⁴ General agreement, to within a factor of 2, is found among the various determinations, at all molar volumes throughout the bcc phase. The dependence of J on molar volume is also in fair qualitative agreement with theory.

The situation with regard to dilute solid mixtures of He^4 in He^3 is less clear. While pressure-vs-temperature, susceptibility-vs-temperature, and relaxation-time measurements have been performed on such dilute mixtures, a consistent interpretation of all the experimental data appears to be lacking. The presence of He^4 strongly affects the He^3 nuclear relaxation times.^{40,43-46} As reviewed by Guyer *et al.*,⁵¹ the effects can be accounted for by the presence of $\text{H}_x^{3,4}$ in the total exchange Hamiltonian. Bernier and Landesman, however, have pointed out that the effects can also be explained with enhanced exchange.^{45,46}

Henricksen, Pancyzk, and Adams⁴¹ have measured P vs T for several dilute He^4 - He^3 mixtures and molar volumes, and to within the accuracy of their experiment they found no effects due to the He^4 impurity.

Recently two studies of the effects of dilute He^4 on the temperature dependence of the susceptibility have been performed. The first was that of Cohen, Pipes, Verosub, and Fairbank.³² They observed large deviations from Curie-Weiss law behavior in some cases, and Curie-Weiss law with very large values of the Weiss constant, of both signs, in others. The later measurements of Richards and Homer³³ showed Curie-Weiss behavior, with a Weiss constant of 0 ± 5 mK at all He^4 concentrations and molar volumes, apparently inconsistent with the results of Cohen *et al.*

In this work we have used the technique of nuclear magnetic resonance to reexamine the temperature dependence of the nuclear magnetization of dilute solid mixtures of He^4 in He^3 in the bcc phase. Measurements were performed at four He^4 concentrations ranging from 3.5×10^{-5} to 2.0×10^{-2} . The purest sample was measured at 21, 22, 23, and 24 cm^3/mole , while the other mixtures were measured at 21 and 23 cm^3/mole . The temperature range for the measurements was 0.95 to 0.32 K.

The recent measurements of the susceptibility of pure solid He^3 by other groups^{37-39,42} were all performed down to temperatures below 40 mK. The pressure measurements³¹ and melting-curve work³⁵ were also very-low-temperature experiments. The temperature region below 300 mK is characterized by high thermal impedances, leading to long thermal relaxation times; and also by long longitudinal relaxation times. These effects might possibly lead to errors in thermometry, due to poor thermal contact and to saturation in the nu-

clear spin system during NMR measurements. These problems are present to a much smaller extent above 300 mK. The present work serves as a high-temperature check on the lower-temperature experiments. It also provides additional and more accurate data on the effects of He^4 on solid He^3 through a study of changes in the Weiss constant due to the presence of the impurity. In particular, the apparent inconsistency between the results of Cohen *et al.*³² and those of Richards and Homer³³ is carefully reexamined. To our knowledge, the susceptibility measurements in He^3 - He^4 mixtures reported here are the most accurate of their kind available.

II. EXPERIMENTAL TECHNIQUE

A. Refrigeration

Much of the cryogenic equipment was of conventional design with well-known techniques used to minimize the heat leak into the cryogenic regions. Sample refrigeration was achieved by pumped He^4 and He^3 refrigerators which attained temperatures of 1.0 and 0.3 K, respectively. The apparatus in the vicinity of the sample chamber is shown in Fig. 1. The sample chamber was machined from nylon, with the sample region having an i. d. of 0.052 in. and an internal length of 0.5 in. The exterior of the chamber was provided with a small groove which served as the form for the NMR coil producing the \vec{H}_1 field. The chamber was screwed onto a threaded copper fitting on the inside wall of a

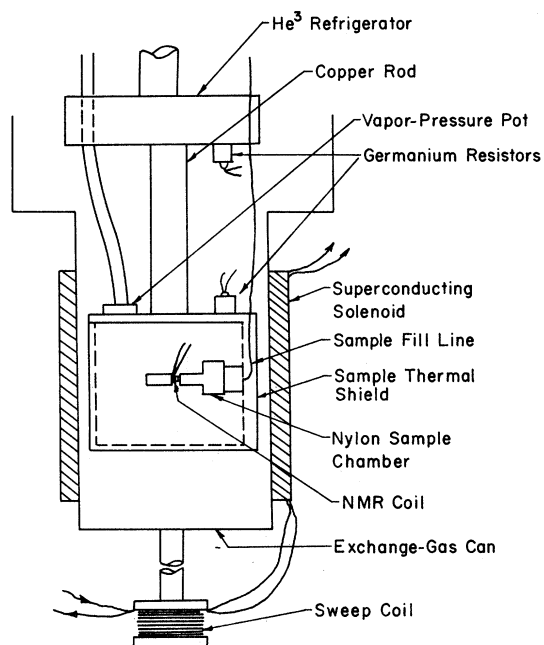


FIG. 1. Details of the apparatus in the vicinity of the sample chamber.

copper support can which acted as a heat shield. The can was connected to the He^3 refrigerator by a solid copper bar 15 in. long and $\frac{1}{2}$ in. in diameter. The sample chamber fitting was bored out to receive the fill line.

B. Thermometry

The sample temperature was measured by using two commercial arsenic-doped germanium resistance thermometers (GRT's), one of which was mounted on the He^3 refrigerator, with the other on the top of the sample-chamber support can (see Fig. 1). They were calibrated against the combination of a He^3 -vapor-pressure thermometer, and the nuclear susceptibility of the purest and most dense ($21 \text{ cm}^3/\text{mole}$) solid He^3 sample, by a procedure to be described in what follows.

The GRT's were from two different manufacturers,⁵⁵ and both had a claimed repeatability upon cycling between room temperature and 4.2 K of 0.5 mK. Extensive checks of the repeatability were made on a number of these GRT's by cycling the resistors in a standard liquid-helium storage Dewar on the order of 100 times. Both of the resistors used were repeatable approximately within the quoted range.⁵⁶ The repeatability between room temperature and 0.32 K, however, was only about 1 mK for the sample-can GRT, and much worse for the He^3 -refrigerator GRT. The GRT's were nevertheless usable as temperature standards as long as they were kept below liquid-nitrogen temperature after calibration. Under these conditions, the repeatability at 0.32 K as measured against vapor-pressure thermometry was within 0.1 mK for both over a period of several months.

The resistance-measuring currents used ranged from $1.2 \mu\text{A}$ at 0.95 K to $0.5 \mu\text{A}$ at 0.32 K, and produced heating ranging from 4×10^{-3} to 1×10^{-3} erg/sec, which were observed to have negligible effect on the germanium-sensing-element temperature.

The GRT's were checked for magnetoresistance effects between 0 and 1 kG. An upper bound to the observed magnetoresistance, $\Delta R(H)/R(H=0)$, was 0.05% at 1 kG and 0.35 K. In addition, drifts of one GRT with respect to the other which would represent temperature shifts larger than 0.1% were never observed over the entire range of temperatures used.

A vapor-pressure bulb in the top of the sample support can (Fig. 1) was connected to the room by $\frac{1}{4}$ - and $\frac{1}{8}$ -in. thin-walled stainless-steel tubes, which were thermally anchored at the He^3 refrigerator. These tubes were joined to the vapor-pressure bulb by a common $\frac{1}{4}$ -in. annealed copper tube which extended from below the He^3 refrigerator. The principal vapor-pressure-measuring instrument was an MKS Baratron type-77 differential

pressure meter with two type-77H strain-gauge pressure heads, one with a range from 0 to 30 torr, and the other with a range of 0 to 1 torr. A CVC, GM-100A McLeod gauge was also available.

The He^3 -vapor-pressure gas was analyzed by mass spectrometry⁵⁷ before the beginning of the data collecting, and again afterwards, and found to have a He^4 concentration of less than 0.1%. According to Roberts *et al.*,⁵⁸ this is sufficient to assure a temperature error of less than 0.02% between 1.0 and 0.3 K.

In order to calibrate the GRT's, the nuclear susceptibility of the purest He^3 sample at 21 cm^3/mole was measured as described in Secs. II C and II D, and assumed to follow Curie-Weiss law behavior. The Weiss constant was calculated from Eq. (4) using the value of $|J|$ measured by Pancyzk and Adams,³¹ and the negative sign for θ measured by Kirk, Osgood, and Garber.³⁹ The Curie constant was evaluated in the temperature region above 0.8 K, where vapor-pressure thermometry could be used without application of a thermo-molecular correction. Lower temperatures were then calculated from the measured susceptibilities.⁵⁹

By repeated measurement of the height of the NMR signal, the thermal relaxation time for establishing equilibrium between the sample and the thermometers was determined to be less than five min at all temperatures used.

C. Susceptibility

The static magnetic susceptibility of the solid- He^3 samples was measured using continuous-wave nuclear-resonance techniques. Determination of values of the Weiss constants with an uncertainty of ± 1 mK or better, from data taken above 0.3 K, required measuring relative susceptibilities to 0.1% or better.

A block diagram of the Rollins-type continuous-wave spectrometer used for detection of the resonance signal is shown in Fig. 2. The tank circuit, tuned to a resonant frequency of 3.54 MHz, had a Q of about 80 and an empty-coil resonant impedance of 2700 Ω . A superconducting solenoid in the persistent mode provided the large field, \vec{H}_0 , at the sample. The measured field homogeneity during operation was 0.02%/cm. Further inhomogeneity was provided by two large coils wound on the exterior of the Dewar and powered by a stable dc supply. The \vec{H}_0 field could be swept over a limited range, by means of a small superconducting sweep solenoid, which was part of the same closed loop as the main solenoid (see Fig. 1). A 1-G change in \vec{H}_0 was produced per ampere of current in the sweep solenoid.

A phase-locked rf oscillator in series with a 1-M Ω ceramic resistor provided a constant-current source for the tank. The rf frequency drifted typ-

ically less than 1 Hz out of 3.54 MHz during a run, but the amplitude often drifted on the order of 0.5%. The rf voltage across the tank was amplified by a low-noise preamplifier built after the design of Clark.⁶⁰ The total gain of the amplification chain was 1.6×10^4 . The amplified signal was rectified and filtered with a resultant bandwidth of about 10^4 Hz. The rectified rf voltage was monitored continuously. The detected nuclear-resonance signals were averaged 64 times for each point by a Fabritek model-1061 signal-averaging computer (SAC), which had a 1024-channel memory. The \vec{H}_0 field sweep, and hence the resonance signal, was synchronized with its memory address system.

Extraction of a measure of χ_0 (the static nuclear susceptibility) from the measured voltage signal, with the precision needed in this experiment, required careful attention to tank-circuit analysis, measured line shape details, and nonlinearities and calibration of the spectrometer.

Bruce, Norberg, and Pake⁶¹ early pointed out the difficulty of obtaining resonance signals in a Rol-

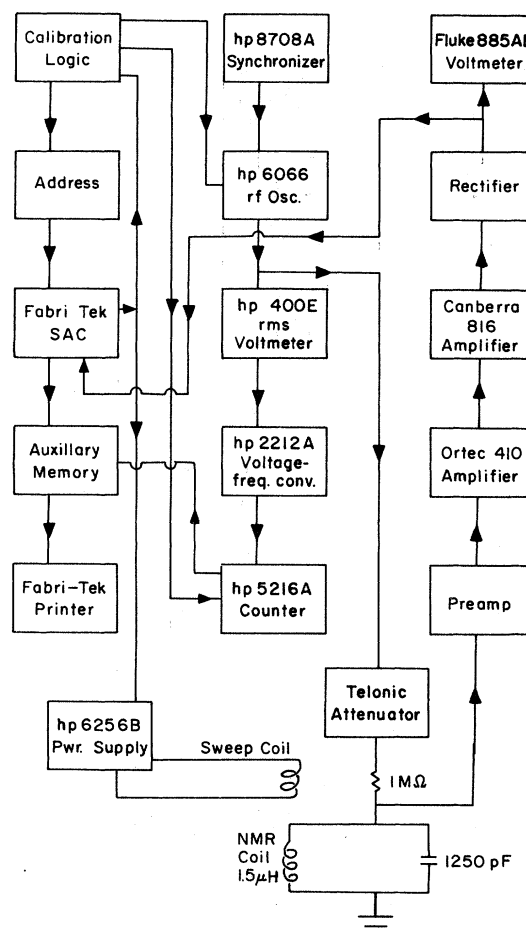


FIG. 2. Block diagram of Rollins-type spectrometer.

lins spectrometer of purely absorptive nature in situations requiring large signal amplitudes. An analysis was made of the circuit used in the present work in order to investigate possible higher-order corrections to the tank voltage than are usually calculated.²⁵ The result is that the usual results are valid provided that the voltage applied at the tank has a frequency $\omega_a = \omega_r + \Delta\omega$, where ω_r is the resonant frequency of the actual circuit, and $\Delta\omega$ is given by

$$\Delta\omega/\omega_r = [Q_0^2 + 2]^{-1}, \quad (5)$$

where Q_0 is $\omega_0 L/R$, ω_0 being the resonant frequency of the equivalent parallel circuit.⁶² In this case, assuming that for an inductor enclosing a material with susceptibility χ , one can write $L = L_0(1 + 4\pi\chi)$ (see Appendix), and also that $\chi = \chi' - i\chi''$ the rectified voltage across the tank driven by a constant amplitude current source is very close to

$$|v| \approx \frac{|v_0|}{(1 + 4\pi Q_0 \chi'')} \left(1 - \frac{1}{2} \frac{(4\pi Q_0 \chi')^2}{(1 + 4\pi Q_0 \chi'')^2} \right), \quad (6)$$

where $|v_0|$ is the voltage drop across the empty coil. If ω differs from ω_a , a term linear in χ' is mixed into the signal $|v|$. For small frequency differences, this is seen as a base line offset in the resonance signal, and experimentally ω_a was selected by matching baselines.

Defining $\Delta|v| = |v_0| - |v|$, it is easily seen that

$$\frac{\Delta|v|}{|v|} \approx 4\pi Q_0 \chi'' + \frac{1}{2} \frac{(4\pi Q_0 \chi')^2}{(1 + 4\pi Q_0 \chi'')^2}. \quad (7)$$

Thus, for a point on the resonance line for which $\chi' = 0$,

$$\Delta|v|/|v| \approx 4\pi Q_0 \chi'', \quad (8)$$

which, for $|\Delta L|/L_0 \leq 0.01$, is accurate to a part in 10^4 or better. Equation (8) and the fact that χ'' is proportional to χ_0 was the basis for our data reduction.

In order to accurately measure the relative height⁶³ of the averaged resonance line, a precise calibration of the spectrometer was made for each sweep through the resonance. This allowed corrections to be made for short- and long-term gain drifts in the amplifier chain, fluctuations in the applied rf level, and nonlinearities in the calibration itself. The calibration was accomplished by step modulating the amplitude of the oscillator output after each sweep through the line. The amount of modulation was adjusted so that the height of the step was as close as possible to the height of the resonance signal. The modulation step occupied approximately the last 50 channels of the SAC memory. The output of the oscillator was measured by a digital rms voltmeter at the point just before the modulation, and again at the top of the modulation

step. The digitized voltages of the oscillator before and after modulation were additively stored in a specially built auxiliary two-channel memory. The calibration calculated from the differences in the summed voltages before and after the modulation step, together with the height of the step in the SAC memory, was then used to calculate the height of the resonance line.

The digital rms voltmeter, consisting of a Hewlett Packard 400E rms voltmeter, 2212A voltage-to-frequency converter, and 5216A frequency counter, was calibrated against a Ballantine model-393 high-frequency transfer voltmeter, with a quoted accuracy of 0.02% between 1- and 2-V rms input. This was checked in turn against a dc voltage known to an accuracy of a part in 10^5 , and its nonlinearity was found to be less than two parts in 10^4 .

The calibration accounted for any rf level or gain changes occurring in more than 4 secs. Fluctuations in shorter times were observed to be negligible.

D. Data Analysis

The amplitude of the rf voltage, v_0 , applied to the tank and the rate of field sweep, dH_0/dt , were determined by requiring a signal-to-noise ratio of 1000:1, without saturating the spin system. The field inhomogeneity across the sample, ΔH_0 (artificially broadened by external coils) was set so that the line shape contained a small reference structure, used as described in the following. The experimental parameters satisfying these requirements and selected for all runs of this experiment were an rf level of $\frac{1}{8}$ mV, peak to peak (providing an H_1 field of 4×10^{-4} g); a dH_0/dt of 0.5 G/sec (corresponding to a SAC memory advance rate of 500 channels/sec); and a ΔH_0 of 50 mG. In addition, the delay time between the end of one sweep and the beginning of the next was set at 2.5 sec, which was sufficiently long for H_0 to relax to its pre-sweep value, and the calibration time (time between the unmodulated and modulated carrier voltage measurements) was set between 3 and 4 seconds, which was long enough to allow for the damping of transients. The amplitude of the H_0 field sweep was one gauss.

The value of dH_0/dt used was greater than $2/\gamma T_1 T_2$ for all samples studied, and as shown in Fig. 3, our observed line shapes were not those characteristic of adiabatic slow passage. The details of the line shape varied with changes in dH_0/dt , ΔH_0 , and sample molar volume. In order to properly identify the $\chi' = 0$ point on the line, and to avoid spurious experimental results due to unavoidable variations in H_1 , dH_0/dt , and ΔH_0 , as well as temperature- and density-dependent changes in the relaxation times, T_1 and T_2 , it was necessary to

investigate the origins of our observed line shapes.

Calculations of resonance line shapes for resonance times short compared to relaxation times have been worked out for the case of no field inhomogeneity.⁶⁴ The effect of field inhomogeneity on adiabatic slow-passage lines has also been treated.⁶⁵ The general problem for short resonance times and large field inhomogeneities, however, has not, to our knowledge, been published.

A procedure for calculating observed line shapes under these more general conditions is given in the Appendix. It is shown there that the inductance of the rf coil containing the sample can, to a good approximation, be written as $L = L_0(1 + 4\pi\chi)$ even in

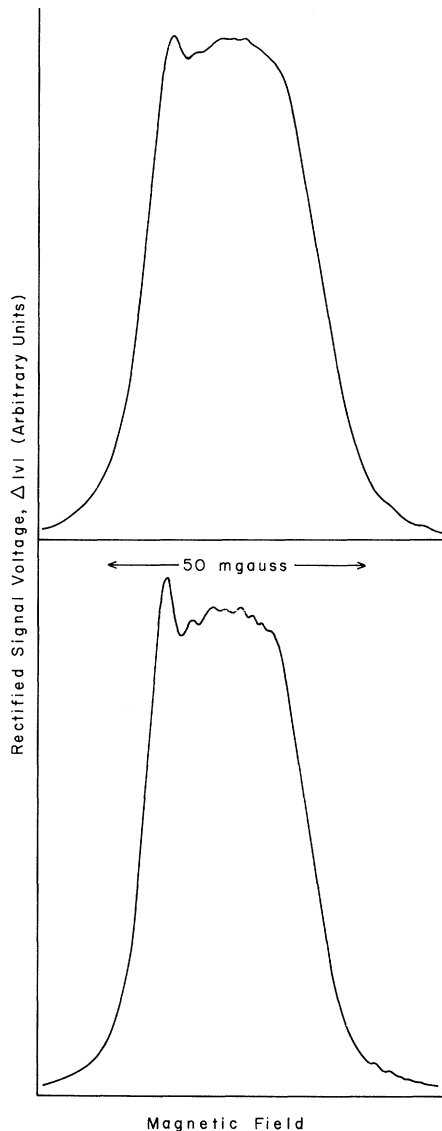


FIG. 3. Observed line shapes. The top resonance line was taken at $21 \text{ cm}^3/\text{mole}$ and the bottom at $24 \text{ cm}^3/\text{mole}$.

the case where $dH_0/dt \geq 2/\gamma T_1 T_2$, and the field inhomogeneity over the sample, ΔH_0 , is large compared to the natural linewidth. χ is given by Eq. (A6a). It is essentially the volume integral of the magnetization per unit volume, divided by the volume integral of the H_1 field. Its real and imaginary parts, both of which are proportional to χ_0 , have time dependences which are not simply related to one another. A given set of experimental conditions (e. g., coil geometry, $H_0(\vec{r}, t)$, $\vec{H}_1(\vec{r}, t)$, T_2 , sample distribution, etc.) determines the time dependence of χ , and thus the resonance line shape, as calculated from Eq. (6).

As described in the Appendix, values for $\chi(t)$ were calculated by numerical techniques for a model set of experimental parameters. The observed qualitative agreement between the model and experimental line shapes under a variety of experimental parameters leads to the belief that the straightforward calculations in the Appendix are valid.

If χ is written

$$i\chi = \chi'' + i\chi' \equiv -\gamma H_0 \chi_0 [I''(t) + iI'(t)], \quad (9)$$

and if for some time t' ,

$$\chi'(t') = 0, \quad (10)$$

then clearly

$$\chi''(t') = \gamma H_0 \chi_0 I''(t'). \quad (11)$$

Thus, for clarity only the point where $\chi' = 0$ is defined by a time t' during resonance. Then Eq. (8) gives

$$\Delta |v| / |v| = -4\pi Q_0 \omega_0 \chi_0 I''(t'). \quad (12)$$

During a run, $-4\pi Q_0 \omega_0 I''(t')$ is constant and temperature independent,⁶⁶ so

$$\Delta |v| / |v| \propto \chi_0. \quad (13)$$

Calculations showed that the $\chi' = 0$ point could be far from the top of the resonance line. The contribution to the height of points on the line (each point being a channel in the SAC memory) due to $\chi' \neq 0$ was roughly proportional to $1/T^2$. These points grew faster with decreasing temperature than the point at which $\chi' = 0$. Thus, comparing successive points in the lines at the highest and lowest temperatures of a run, or reducing the data at several points on the line and using the point with the most negative value of θ , provided an experimental method of identifying the $\chi' = 0$ point. Identifying corresponding points on all of the lines making up one run was accomplished by using the detailed structure of the line itself as a reference frame. It was found that points on the line defined by three adjacent channels near the middle of the top of the line all gave the most negative values of θ , within experimental error. This result was in

the same place for all the lines under all conditions of the experiment. The reduced data reported in what follows was always taken from the point in the middle of this region.

With the $\chi' = 0$ point determined, from Eqs. (3) and (13),

$$T = \frac{C'}{\Delta|v|/|v|} + \theta, \quad (14)$$

where $C' \propto C$. Thus, best values of θ were found by fitting T vs $1/[\Delta|v|/|v|]$ to a straight line. For this purpose, the best-fit equations of Kermack and Haldane⁶⁷ appropriate to the case of equal error in ordinate and abscissa were used.

E. Sample

The gas for the purest He³ samples was purchased from Mound Laboratories. All of the impure samples were mixed from this gas in a gas-handling system which was similar in design to that used by Fairbank and Walters²¹ and by Adams, Meyer, and Fairbank.²²

After data collection on the purest sample was completed, it was mixed with a calculated amount of He⁴ in a Toeppler pump to make the first impure sample. Each succeeding impure sample was mixed from the preceding sample by addition of more He⁴. The He⁴ added was cleaned in a liquid-helium trap before mixing, and special care was taken to ensure thorough mixing. The mixed sample was again cleaned in a helium trap. The concentrations of all the samples were measured by mass spectrometry,⁵⁷ with the sample for analysis being drawn off immediately after completion of the susceptibility measurements. The resulting concentrations of He⁴ in He³ were 3.7×10^{-5} , 3.2×10^{-4} , 2.9×10^{-3} , 2.0×10^{-2} , respectively. As a check, the last mixture was analyzed both before and after taking data, with a resulting concentration measurement of 2.1×10^2 before the runs, and 1.88×10^2 afterwards. Based upon this, a conservative estimate of the error in the concentration determination is 20%.

Solidification of the sample was observed by sitting on the NMR line (i. e., adjusting H_0 to ω_0/γ) with a rf voltage level sufficiently large to partially saturate the signal in the liquid. As T_1 is much shorter in the solid than the liquid, the solid saturates much less, and formation of solid was indicated by growth of the NMR line. When the line ceased growing, solidification was complete.

Attempts made to grow the sample by the often-used blocked-capillary technique failed because of plug slippage. For this reason, all of the crystals in this work were grown at constant pressure and temperature, rather than constant molar volume. The sample temperature, determined from the He³-vapor pressure, or for the most dense solid, the

vapor pressure of the He⁴ bath, was set equal to the melting temperature T_m , and the sample pressure was set about 1 atm below the melting pressure P_m . T_m and P_m were determined from the phase diagrams.⁶⁸ Fifteen to twenty minutes were allowed to establish thermal equilibrium in the sample.

In order to prevent supercooling and blockage of the fill capillary during gradual pressurization, the sample pressure was suddenly increased from 3 to 5 atm beyond P_m , which appeared to seed the crystal growth. The pressure was then lowered to P_m , and the solid was observed to form rapidly at the constant temperature T_m . It was possible to tell whether the sample line was open by giving a rapid 1-atm increase in sample pressure, which produced a disturbance in the sample region that was detected as a dip in the resonance signal.

Once the resonance signal had ceased growing, a check was made to assure that the fill line was open. The solid was allowed to anneal for 1 h with the temperature set 2–3 mK below T_m . Then, if the resonance signal still indicated an intact solid, the temperature was lowered and the pressure raised to several atmospheres above P_m so that the He³ would freeze high in the fill line.

Due to the method used to seed crystallization and to slow drifts (approximately 1 atm per 5 min) in the pressure applied to the sample during the solidification, the pressures that the solids were formed and annealed under was $P_m \pm 1$ atm. This results in an uncertainty in molar volumes of about ± 0.1 cm³/mole at 24 cm³/mole, the worst case. For the low concentrations of He⁴ used, the phase diagram of the mixtures was essentially identical to that of the pure solid.⁶⁹ No corrections were applied.

F. Data Collection

Measurements of the NMR signal as a function of sample temperature and molar volume were carried out in all of the samples described above. The measurements on the pure (He⁴ concentration = 3.7×10^{-5}) He³ at 21 cm³/mole were used to establish the primary temperature scale, as already described. The order of the data collecting was as follows. First, five runs were made at 21 cm³/mole in the pure sample, followed by five runs at 22 cm³/mole and six runs each at 23 and 24 cm³/mole. These were followed by seven more runs at 21 cm³/mole to check for drifts in the temperature scale. (The time between the initial 21-cm³/mole runs and the final 21-cm³/mole runs was about eight weeks.) Then three runs each at 21 and 23 cm³/mole were made on each of the three mixtures, in order of increasing He⁴ concentration. (These measurements required 2 weeks.)

Each run commenced with zeroing and calibrat-

ing the digital rms voltmeter against a standard cell traceable to NBS and against the Ballantine high-frequency transfer voltmeter. The Baratron heads were zeroed, and the rf frequency adjusted to give zero base line offset in the resonance signal. The value of H_0 was adjusted to center the resonance signal in the SAC memory.

The temperature points at which resonance line measurements were made were chosen during the first run at approximately 50 mK intervals, as estimated by the vapor pressure. The resistances of the GRT's were recorded against these vapor pressures. The temperature points of all of the other runs were then determined by the resistance of the sample can GRT.

The sample was cooled to the first temperature point as indicated by the sample-can GRT, and with the He³ refrigerator stabilized, the vapor pressure was recorded. The temperature was thereafter kept stable by reference to this vapor pressure, permitting recording of the He³-refrigerator GRT, and setting of the modulation level of the oscillator necessary for calibration, as discussed previously.

Five minutes were always allowed to pass between the initial temperature stabilization and the beginning of the resonance-signal measurement. After this interval, the SAC was started, and automatically stopped after 64 sweeps. While the memory was being printed out, the sample was cooled to the next temperature. All of the successive points were taken as just described, except that several times during the first few runs, many points were taken at each of a number of temperatures, in order to check for reproducibility.

After the point at the lowest temperature was completed, the sample was warmed by means of a manganin-wire heater wrapped on the copper rod between the sample can and He³ refrigerator. Upon warming, additional data points were taken at four or five temperatures, including the temperature at which the run started. Comparison of the first and last points allowed a check for long-term drifts.

The starting temperatures for each run varied with molar volume in order to avoid the region of strongly temperature dependent T_2 just below the melting temperature. The 21, 22, 23, and 24 cm³/mole runs were started at 0.95, 0.90, 0.85, and 0.73 K, respectively. Below these temperatures T_2 becomes approximately constant,⁵¹ and this was the region in which data were taken. Extra temperature points were included in the 23 and 24 cm³/mole runs to compensate for the reduced temperature interval of measurement. The total number of points in each run varied from 17 to 21.

As discussed earlier, use of Eq. (14) to determine a temperature scale required knowing C' .

This was evaluated from temperatures determined by vapor-pressure thermometry in the region above 0.8 K, where the vapor pressures were accurate without recourse to thermomolecular corrections. For all the temperature-scale runs, two to four data points (one data point equals one SAC-averaged resonance line) were taken at each of the four temperatures 0.800, 0.850, 0.900, and 0.950 K. For each data point the value of C' was determined from Eq. (14) together with the value of θ obtained by Panczyk and Adams,³¹ and these were averaged together. The averaged C' was then used to determine the values of T for all of the other temperatures at which data was taken. The final temperature scale was an average of the scales determined from each of the runs. Since a quadratic contribution of χ' to the line height would make the temperature too small, the $\chi' = 0$ point for these runs was determined as that point which gave the highest temperature at the low end of the scale.

III. RESULTS, DISCUSSION, AND CONCLUSION

A. Pure He³

The data for the runs in the purest sample are given in Table I. The labeling of the runs for each molar volume corresponds to the order in which the data were taken. For each run, the best-fit values of the intercept θ and the slope C' are shown, in addition to the rms perpendicular distance of the data from the best-fit line. For purposes of computing this rms distance, $[\Delta|v|/|v|]^{-1}$ was normalized to T at the highest temperature for each run so that equal weights would be given to the ordinate and abscissa. The average intercept for each molar volume, $\langle\theta\rangle$, is given, along with the standard deviations of the θ 's. The average intercept and the standard deviations from that average were computed from the list of intercepts obtained from each run for a given molar volume. The average values of the slopes are also included. The average slopes scale with T_2 in the manner predicted by the model line shape, if correction is made for the change in filling factor with molar volume.

The values of $\langle\theta\rangle$ are compared with the results of other groups in Fig. 4. The solid line was calculated from Eq. (4), using the exchange energies of Panczyk and Adams³¹ measured at very low temperatures. The data of Kirk *et al.*,³⁹ as well as our own, were taken very close to 21, 22, and 24 cm³/mole, and the separation of the data points at these molar volumes is only for clarity. The separation at 23 cm³/mole is real. Data taken close to 24 cm³/mole by Anderson, Reece, and Wheatly⁴² and by Sites, Osheroff, Richardson, and Lee³⁸ have been omitted from Fig. 4, in order to avoid crowding at the low-density end. Their points fell near the Panczyk and Adams line.

The inclusion of the 21-cm³/mole data in Table I

TABLE I. Results of runs in pure (3.7×10^{-5} He⁴) solid He³ at 21, 22, 23, and 24 cm³/mole. The 21-cm³/mole data is included as a check on the data which made up the temperature scale.

Run	θ (mK)	Slope (C')	rms perpendicular distance from best fit ($\times 10^{-4}$)
21/I	-0.77	0.1440	7.8
21/II	0.79	0.1435	5.8
21/III	0.23	0.1436	5.3
21/IV	-0.05	0.1440	4.2
21/V	0.97	0.1453	8.5
21/VI	-0.68	0.1454	8.4
21/VII	-1.49	0.1436	7.7
21/VIII	-1.20	0.1434	5.7
21/IX	-1.33	0.1443	7.3
21/X	0.17	0.1437	6.4
21/XI	0.15	0.1439	7.8
21/XII	0.36	0.1437	5.7
$\langle\theta\rangle = -0.24$ mK; $\sigma_\theta = 0.82$ mK; $\langle C'\rangle = 0.1440$			
22/I	-0.45	0.1414	5.1
22/II	-2.66	0.1416	6.3
22/III	-0.05	0.1390	7.1
22/IV	-0.45	0.1402	3.7
22/V	-1.53	0.1404	4.0
$\langle\theta\rangle = -1.03$ mK; $\sigma_\theta = 1.06$ mK; $\langle C'\rangle = 0.1405$			
23/I	-1.12	0.1359	4.5
23/II	-1.95	0.1356	4.3
23/III	-1.41	0.1364	6.6
23/IV	-1.54	0.1382	4.0
23/V	-1.48	0.1377	2.5
23/VI	-1.41	0.1375	4.9
$\langle\theta\rangle = -1.49$ mK; $\sigma_\theta = 0.27$ mK; $\langle C'\rangle = 0.1369$			
24/I	-3.78	0.1328	5.9
24/II	-3.72	0.1322	3.2
24/III	-1.96	0.1318	5.5
24/IV	-2.55	0.1322	4.3
24/V	-3.77	0.1327	5.3
24/VI	-2.64	0.1320	4.1
$\langle\theta\rangle = -3.07$ mK; $\sigma_\theta = 0.78$ mK; $\langle C'\rangle = 0.1323$			

and Fig. 4 is not meant to indicate that these measurements are representative of new values of θ . Rather, the value of $\langle\theta\rangle$ given confirms that this temperature scale was self-consistent.

Figure 4 shows that the accuracy in θ of the present high-temperature work is competitive with the measurements at much lower temperatures, and thus provides confirmation of both sign and magnitude of θ . The volume dependence of θ agrees quite well with that determined by Kirk *et al.*,³⁹ and that calculated from the exchange energies of Panczyk and Adams.³¹

B. Dilute Mixtures of He⁴ in He³

The data for the dilute mixtures of He⁴ in He³ are shown in Table II. The quantities listed are the

same as for the pure-He³ data of Table I. The average values of θ for each sample including those for the purest mixtures discussed above all have standard deviations on the order of 0.5 mK. The values of $\langle\theta\rangle$ are consistent with the measurements of Richards and Homer,³³ who interpreted their data as placing a value of 0 ± 5 mK on θ for all of their samples at every molar volume measured.

Comparison of Tables I and II shows that the scatter in the data for the mixture runs is about the same as for the pure runs. The values of $\langle\theta\rangle$ for the 23-cm³/mole solids at all three He⁴ concentrations are seen to be essentially the same as that measured for the pure solid within one standard deviation. Indeed, if the $\langle\theta\rangle$'s for all of the 23-cm³/mole runs are averaged together, the result is -1.44 mK, as compared with the value of -1.49 mK for the purest solid.

The data at 21 cm³/mole, however, suggests a small shift of $\langle\theta\rangle$ in the ferromagnetic direction, which appears to be statistically significant. As

TABLE II. Results for runs in dilute solid mixtures of He⁴ in He³ at 21 and 23 cm³/mole. Runs labeled A, B, and C are at He⁴ concentrations of 3.2×10^{-4} , 2.9×10^{-3} , and 2.0×10^{-2} , respectively.

Run	θ (mK)	Slope (C')	rms perpendicular distance from best fit ($\times 10^{-4}$)
21A/I	0.22	0.1435	6.6
21A/II	0.06	0.1437	7.0
21A/III	-1.12	0.1437	10.2
$\langle\theta\rangle = -0.28$ mK; $\sigma_\theta = 0.73$ mK; $\langle C'\rangle = 0.1437$			
23A/I	-1.56	0.1354	5.3
23A/II	-1.77	0.1355	5.6
23A/III	-2.25	0.1362	6.8
$\langle\theta\rangle = -1.86$ mK; $\sigma_\theta = 0.35$ mK; $\langle C'\rangle = 0.1357$			
21B/I	0.85	0.1436	7.0
21B/II	1.06	0.1434	4.5
21B/III	1.42	0.1433	5.5
$\langle\theta\rangle = 1.11$ mK; $\sigma_\theta = 0.29$ mK; $\langle C'\rangle = 0.1434$			
23B/I	-0.80	0.1351	4.9
23B/II	-0.95	0.1351	6.0
23B/III	-2.36	0.1352	5.5
$\langle\theta\rangle = -1.37$ mK; $\sigma_\theta = 0.86$ mK; $\langle C'\rangle = 0.1351$			
21C/I	0.63	0.1413	6.0
21C/II	1.80	0.1410	5.0
21C/III	1.68	0.1407	7.1
$\langle\theta\rangle = 1.37$ mK; $\sigma_\theta = 0.64$ mK; $\langle C'\rangle = 0.1352$			
23C/I	-0.47	0.1352	5.6
23C/II	-1.38	0.1353	5.1
23C/III	-1.08	0.1352	2.8
$\langle\theta\rangle = -0.98$ mK; $\sigma_\theta = 0.46$ mK; $\langle C'\rangle = 0.1352$			

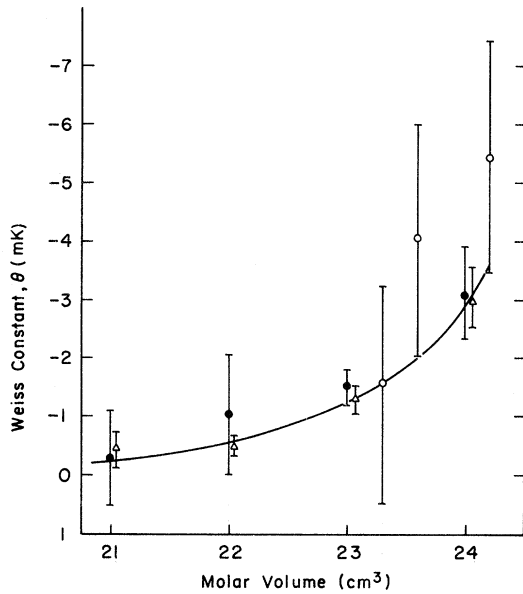


FIG. 4. Plot of measured Weiss constant of pure solid He^3 vs molar volume. A comparison of our results with other recent magnetic susceptibility and pressure data. ●, results listed in Table I, this paper. ○, results from Ref. 37. △, results from Ref. 39. Solid line indicates results from Ref. 31.

seen in Table II, there is no overlap between the standard deviations for θ at the two lowest He^4 concentrations, and those of the two highest. The measured values of θ do, however, overlap to within two standard deviations.

With difficulty, this shift in $\langle\theta\rangle$ could be explained by a shift in the temperature scale such that the temperatures measured were higher than the actual temperature of the sample. Such a shift would have been undetected in the event that both of the GRT's calibrations as well as the vapor-pressure measurements had shifted by just the right amounts so that they would all be consistent relative to each other, yet still all indicate the wrong temperature. While such an occurrence is possible, it is highly improbable.

Alternatively, the GRT on the sample support can (GRT_2) could have shifted relative to the other GRT (GRT_1) and the vapor-pressure measurements. In order for the sample temperature to be colder than measured by GRT_2 , for a given GRT_2 value, GRT_1 would have to read greater than usual, and the vapor pressure would have to be less than usual. In fact, no such shift of GRT_1 relative to GRT_2 was seen, within a $\pm 3 \Omega$ scatter (equivalent to ± 0.2 mK at 0.32 K). Also, the only shift in vapor-pressure measurements observed between the period of the second set of temperature-scale-determining runs in the pure solid, and the runs in dilute mixtures, was an approximately $0.04\text{-}\mu$ shift to higher vapor pres-

ures (0.12 mK at 0.32 K), which is in the wrong direction to account for the necessary temperature-scale shift. While it is felt that the thermometry remained accurate during the runs in the $\text{He}^3\text{-He}^4$ mixtures, a final check of the temperature scale at the end of all the runs, in order to verify the thermometry accuracy was planned but could not be carried out owing to experimental difficulties.

The lack of a final temperature-scale check, together with the relatively small number of runs used to establish the standard deviations in Table II, lead to the conclusion that the observed shift in $\langle\theta\rangle$ is only suggestive of effects intrinsic to $\text{He}^3\text{-He}^4$ mixtures, and should be interpreted as providing an upper limit to a He^4 -dependent θ shift.

As indicated in the Introduction, the effects of the He^4 impurity on the properties of the solid- He^3 system can be described by including an enhanced exchange term and an isotope exchange term, in the total system Hamiltonian. Using a Hamiltonian containing both exchange terms, Eqs. (1) and (2), but no exchange enhancement, Balakrishnan and Balakrishnan¹⁹ have recently calculated an expression for $\theta(x)$, which is Eq. (16) here, where x is the atomic fraction of He^4 . In this model, J'' , the $\text{He}^3\text{-He}^4$ hopping frequency, plays no role in determining θ .

Bernier⁴⁴ has considered a Hamiltonian with only the enhanced Heisenberg term present (in addition to the unenhanced term), and from the partition function for an isotopic mixture of solid helium, he calculates the He^4 dependence of θ in the limit $T \gg \theta$, and to first order in He^4 concentration, as

$$\theta(x) = \theta_0 \{1 + x[14(J_e/J) - 53]\}, \quad (15a)$$

where J and J_e are the normal and enhanced exchange energies, respectively, x is the He^4 concentration, and θ_0 is the value of θ at $x=0$. Richards and Homer,³³ using molecular field theory, arrive at a similar expression:

$$\theta(x) = \theta_0 \{1 + x[14(J_e/J)]\}. \quad (15b)$$

Both (15a) and (15b), however, exhibit anomalous behavior in the limit $J_e \rightarrow J$, where one would expect that

$$\theta(x) = \theta_0(1 - x). \quad (16)$$

This anomaly in Eq. (15b) can be traced⁷⁰ to the expression for χ_0 of Richards and Homer. The origin of that in Eq. (15a) is found in the assumption that $J_e/J \gg 1$, which was used in its derivation. A linear dependence of θ upon x is reasonable, however in the region where x is small enough. An intuitively appropriate form of $\theta(x)$ in the dilute- He^4 region is thus taken to be

$$\theta(x) = \theta_0(1 + Kx), \quad (17)$$

which incorporates Eqs. (15a), (15b), and (16).

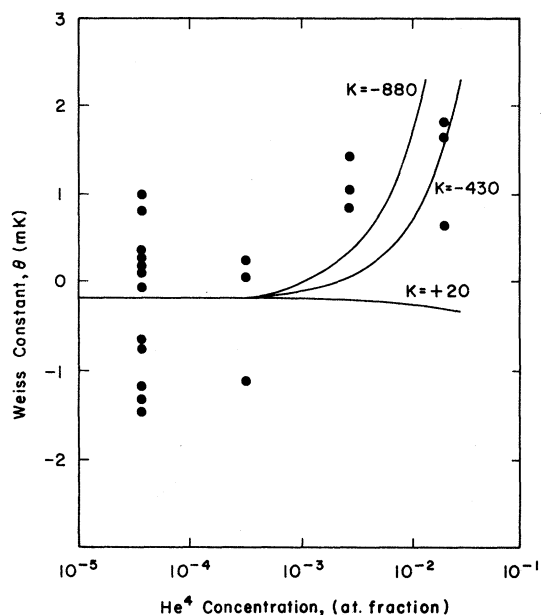


FIG. 5. Plot of measured Weiss constant vs concentration of He⁴ at 21 cm³/mole. Each point represents a single run. The solid lines are the equation $\theta = \theta_0(1 + Kx)$ for $K = -880, -430, \text{ and } +20$, and $\theta_0 = -0.20$ mK.

The exact nature of K and its dependence on J_e/J is dependent upon the details of the model assumed for the localized lattice strain produced by the impurity and will not be pursued here. K is taken to be a parameter dependent upon molar volume.

The data listed in Table II are plotted in Figs. 5 and 6 for the 21- and 23-cm³/mole solids, respectively. A least-squares fit of the 21-cm³/mole data to the equation $\theta(x) = a + bx$ with no error assumed in x yields the values $a = -0.20$ mK, with a standard deviation of 0.20, and $b = 86.1$, with standard deviation 25.7.⁷¹ The value of a and that of θ_0 , which was assumed to be -0.25 mK for purposes of establishing a temperature scale, are in agreement within one standard deviation. They are also in good agreement with the value of $\langle \theta \rangle$ for the purest sample listed in Table I indicating self-consistency. Using the equation $\theta(x) = (-0.20 \pm 0.20) + (86.1 \pm 25.7)x$ and Eq. (17), a value for K of -430 ± 450 ⁷² is obtained. Eq. (17) is plotted on Fig. 5 for $\theta_0 = -0.20$ mK and $K = -880, -430, \text{ and } +20$.

A similar analysis of the 23-cm³/mole data of Fig. 6 yields $\theta(x) = (-1.58 \pm 0.14) + (30.7 \pm 15.7)x$. A value for K of -19 ± 10 is obtained. Equation (17) is plotted on Fig. 6 for $\theta_0 = -1.58$ and $K = -29, -19, \text{ and } -9$.

One purpose of these measurements was to check the discrepancy between the results of Cohen *et al.*³² and those of Richards and Homer.³³ Our measured values of $\langle \theta \rangle$ in He³-He⁴ mixtures are consistent with, and an improvement upon, the values of

Richards and Homer. However, the measurements of Cohen *et al.* appear to be inconsistent with both the results given here and the results of Richards and Homer. The reasons for this lack of agreement are not fully known.

ACKNOWLEDGMENTS

The authors gratefully acknowledge many valuable conversations with Dr. Robert V. Lange and Dr. Hugh Pendleton, III.

APPENDIX

This appendix derives a method for calculating NMR line shapes that can be observed under a wide range of experimental conditions including those used in this experiment. In addition, it shows that under certain conditions the expression $L = L_0(1 + 4\pi\chi)$ is appropriate to the case of an inductor filled with a material having a magnetization which is nonuniform and exhibits local time dependence, which differs from point to point in the material.

Faraday's law states that the voltage difference across the ends of an inductor which encloses area A is given by

$$v = -\frac{1}{c} \frac{d}{dt} \int_A \vec{B} \cdot d\vec{A}. \quad (\text{A1})$$

Writing $\vec{B}(\vec{r}, t) = \vec{H}(\vec{r}, t) + 4\pi\vec{M}(\vec{r}, t)$, where $\vec{H}(\vec{r}, t) = \vec{H}_0(\vec{r}, t) + \vec{H}_1(\vec{r}, t)$, and for simplicity assuming a

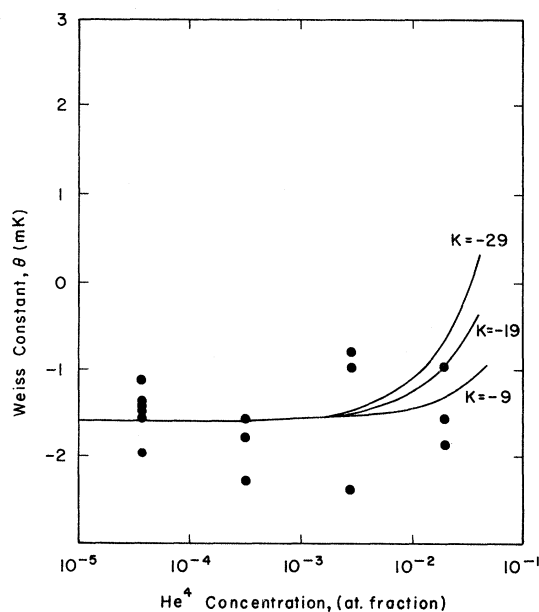


FIG. 6. Plot of measured Weiss constant vs concentration of He⁴ at 23 cm³/mole. Each point represents a single run. The solid lines are the equation $\theta = \theta_0(1 + Kx)$ for $K = -29, -19, \text{ and } -9$, and $\theta_0 = -1.58$ mK.

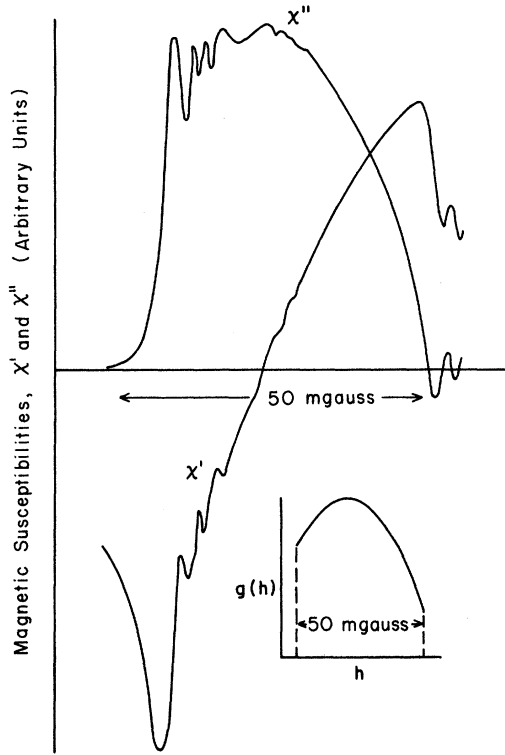


FIG. 7. Plot of calculated magnetic susceptibilities, χ' and χ'' , with $T_2=0.25$ sec, $dH_0/dt=0.1$ G/sec, $h_0=0.05$ G, and $g(h)=N(0.68+1.6h-2.0h^2)$. The inset is a plot of $g(h)$.

coil geometry such that dA is everywhere perpendicular to \vec{H}_0 , a situation appropriate to the present experiment, one obtains

$$v = -\frac{1}{c} \frac{d}{dt} \left[\int_A \vec{H}_1(\vec{r}, t) \cdot d\vec{A} \right. \\ \left. 4\pi i \int_A K(\vec{r}, \omega_0, t) \vec{H}_1(\vec{r}, t) \cdot d\vec{A} \right]. \quad (\text{A2})$$

Here, the result of Jacobssohn and Wangsness⁶⁴ has been used, which states that under general resonance conditions, the magnetization as a function of space, time, and the rf frequency ω_0 can be written

$$i\vec{M} = \vec{M}'' + i\vec{M}' = K(\vec{r}, \omega_0, t) \vec{H}_1(\vec{r}, t) \quad (\text{A3a})$$

with

$$K(\vec{r}, \omega_0, t) = -\gamma \chi_0 H_0(\vec{r}, t) \left\{ \int_{-\infty}^t dt' \exp[-(t-t')/T_2] \right. \\ \left. - i \int_{t_0}^t (\gamma |H_0(\vec{r}, t')| - \omega_0) dt' \right\}. \quad (\text{A3b})$$

Equation (A3b), an integral form of the Bloch equations, depends upon the assumption $M_x \approx M_0$.

The time dependence of $K(\vec{r}, \omega_0, t)$ is due to a beating between precession of the local magnetization and $\vec{H}_1(\vec{r}, t)$. A very simple estimate which

considerably overestimates this time dependence uses the maximum possible beat frequency, $\Delta\omega_0 = \gamma\Delta H_0$, and yields for our experiment

$$\left| \frac{\partial K(\vec{r}, \omega_0, t)}{\partial t} \right| < \Delta\omega_0 |K(\vec{r}, \omega_0, t)| \\ < 10^3 |K(\vec{r}, \omega_0, t)|$$

as $\Delta H_0 = 50$ mG.

Since

$$\left| \frac{\partial H_1(\vec{r}, t)}{\partial t} \right| = \omega_0 |H_1(\vec{r}, t)|,$$

we can then estimate, as $\omega_0 = 2 \times 10^7 \text{ sec}^{-1}$,

$$\left| \int \frac{\partial K}{\partial t} \vec{H}_1 \cdot d\vec{A} \right| < 5 \times 10^{-5} \left| \int K \frac{\partial \vec{H}_1}{\partial t} \cdot d\vec{A} \right|. \quad (\text{A4})$$

Therefore, the term in Eq. (A2) resulting from differentiation of $K(\vec{r}, \omega_0, t)$ with respect to time can be neglected. Further, since the time dependence of $\vec{H}_1(\vec{r}, t)$ is due only to the time dependence in the current $I(t)$ which produces H_1 ,

$$H_1(\vec{r}, t) \equiv I(t) h_1(\vec{r}).$$

Therefore, Eq. (A2) becomes

$$v = -L_0(1+4\pi\chi) \frac{dI(t)}{dt}, \quad (\text{A5})$$

where

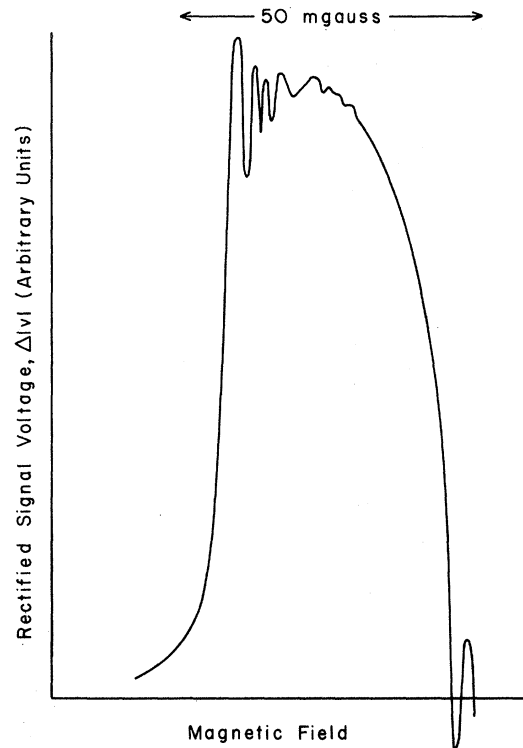


FIG. 8. Calculated resonance line shape obtained from magnetic susceptibilities shown in Fig. 7.

$$i\chi \equiv (cL_0)^{-1} \int_A K(\vec{r}, \omega_0, t) \vec{h}_1(\vec{r}) \cdot d\vec{A} \quad (\text{A6a})$$

and

$$L_0 \equiv c^{-1} \int_A \vec{h}_1 \cdot d\vec{A}. \quad (\text{A6b})$$

Hence, the inductance of the coil can be written in the usual form. Calculation of the real and imaginary parts of χ for a particular set of experimental conditions leads to a knowledge of the line shape.

In order to make use of Eq. (A6a) in the absence of an exact knowledge of the distributions of \vec{H}_1 and \vec{H}_0 across the sample, we assume that $\vec{h}_1(r)$ is constant and that Eq. (A6a) can be written as

$$i\chi = V^{-1} \int_V K(\vec{r}, \omega_0, t) dV, \quad (\text{A7})$$

where V is the volume inside the coil.

As the spatial dependence of $H_0(\vec{r}, t)$ is independent of time while, in the present experiment, its time dependence is linear, we can write

$$H_0(\vec{r}, t) = \omega_0/\gamma + h(\vec{r}) - kt. \quad (\text{A8})$$

Further, as the spatial dependence of $K(\vec{r}, \omega_0, t)$ comes only from the spatial dependence of $H_0(\vec{r}, t)$, we can replace the volume integral above with an integration over h by introducing a weighting function $g(h) dh$, where $g(h)dh$ is defined as the volume

fraction of sample with $h(\vec{r}) = h$. This results in

$$i\chi = -\gamma\chi_0 H_0 \left\{ \int_{-\infty}^t dt' \left[\int_{-\infty}^{+\infty} \exp\left(-\frac{(t-t')}{T_2}\right) - i\gamma k[(t+t')(t-t')] - i\gamma h(t-t') \right] g(h) dh \right\}. \quad (\text{A9})$$

Here, $\vec{H}_0(\vec{r}, t)$ outside the integral in Eq. (A3b) has been replaced by its average H_0 , since the small variations in that quantity contribute very little to the time dependence of χ .

The integration over the field inhomogeneity involves evaluating

$$\int_{-\infty}^{+\infty} e^{-i\gamma h(t-t')} g(h) dh, \quad (\text{A10})$$

where $g(h) = 0$ for h outside the range $0 \leq h \leq h_0$.

This is integrable in closed form for only a small number of functions. Approximating $g(h)$ by a power series of order n ,

$$g(h) \approx N \sum_{k=1}^n b_k h^{k-1}, \quad (\text{A11a})$$

where N is determined by setting

$$\int_{-\infty}^{+\infty} g(h) dh = 1, \quad (\text{A11b})$$

leads to

$$i\chi = -\gamma H_0 \chi_0 \left[\int_{-\infty}^t dt' \exp\left(-\frac{(t-t')}{T_2}\right) - i\gamma k[(t+t')(t-t')] \right] \sum_{q=1}^n q[\gamma(t-t')]^{-1} \{A_q \exp[-i\gamma(t-t')h_0] + B_q\}, \quad (\text{A12a})$$

where

$$A_q = (-i)^q \sum_{j=q}^n b_j h_0^{j-q} \frac{(j-1)!}{(j-q)!} \quad (\text{A12b})$$

and

$$B_q = -(-1)^q (q-1)! b_q. \quad (\text{A12c})$$

Writing $i\chi = \chi'' + i\chi'$, χ'' will receive contributions only from cosine terms for q even, and sine terms for q odd. The inverse is true for χ' . Separate integrals written for χ' and χ'' are solvable by relatively simple numerical techniques.

The evaluation of Eq. (A12a) by three-point Gaussian quadrature, using a CDC-6600 computer, is shown in Fig. 7, with the calculated line shape shown in Fig. 8. The qualitative agreement between Fig. 8 and the experimental line shapes in

Fig. 3 is obvious—the differences are due mainly to uncertainties in $g(h)$.

The detailed structure in both the experimental and calculated line shapes is due to a beating between the time dependence of the magnetization and that of $\vec{H}_1(t)$. The H_0 field inhomogeneity results in different parts of the sample contributing different beat frequencies, which have to be added to give the total structure.

According to this picture, and as seen experimentally and in the model line shape, reduction of T_2 for a given H_0 and ΔH_0 leads to a line with smaller structure. Increasing ΔH_0 for a given dH_0/dt and T_2 has almost the same effect as decreasing T_2 , since the spins dephase more quickly, leading to a rapid damping of the beat signal. Decreasing dH_0/dt for given T_2 and ΔH_0 also decreases the structure.

[†]Work supported in part by the United States Atomic Energy Commission and the Research Corporation.

*Gillette Fellow. Current address: The Department of Physics and Astronomy, Louisiana State University, Baton Rouge, La. 70803.

[‡]Current address: Physics Department, The University of Vermont, Burlington, Vt. 05401.

¹N. Bernardes and H. Primakoff, Phys. Rev. **119**, 968 (1960).

²E. M. Saunders, Phys. Rev. **126**, 1724 (1962); W. J. Mullin, Phys. Rev. **166**, 142 (1968).

³R. L. Garwin and A. Landesman, Physics (N.Y.) **2**, 107 (1965).

⁴D. J. Thouless, Proc. R. Soc. Lond. **86**, 893 (1965).

⁵L. Goldstein, Ann. Phys. (N.Y.) **8**, 390 (1959); Ann. Phys. (N.Y.) **14**, 77 (1961); Phys. Rev. **133**, A52 (1964); Phys. Rev. **159**, 120 (1967); Phys. Rev. **171**, 194 (1968); Phys. Rev.

- 176, 311 (1968); Phys. Rev. **188**, 349 (1969).
- ⁶L. H. Nosanow and G. L. Shaw, Phys. Rev. **128**, 546 (1962).
- ⁷L. H. Nosanow, Phys. Rev. Lett. **13**, 270 (1964).
- ⁸L. H. Nosanow and W. J. Mullin, Phys. Rev. Lett. **14**, 133 (1965).
- ⁹L. H. Nosanow, Phys. Rev. **146**, 120 (1966); J. H. Hetherington, W. J. Mullin, and L. H. Nosanow, Phys. Rev. **154**, 175 (1967); W. J. Mullin, L. H. Nosanow, and P. M. Steinback, Phys. Rev. **188**, 410 (1969).
- ¹⁰L. H. Nosanow and C. M. Varma, Phys. Rev. Lett. **20**, 912 (1968); Phys. Rev. **187**, 660 (1969).
- ¹¹C. M. Varma, Phys. Rev. Lett. **23**, 778 (1969).
- ¹²W. J. Mullin, J. Low Temp. Phys. **4**, 135 (1971).
- ¹³H. R. Glyde, Phys. Rev. **177**, 262 (1969); Phys. Rev. A **1**, 296 (1970).
- ¹⁴R. A. Guyer and L. I. Zane, Phys. Rev. **188**, 445 (1969).
- ¹⁵R. A. Guyer and L. I. Zane, Phys. Rev. Lett. **24**, 660 (1970).
- ¹⁶L. I. Zane, Phys. Rev. Lett. **28**, 420 (1972).
- ¹⁷R. Balakrishnan and R. V. Lange, Phys. Rev. A **3**, 496 (1971).
- ¹⁸R. Balakrishnan and R. V. Lange, J. Phys. (Paris) Suppl. **32**, C1-228 (1971).
- ¹⁹R. Balakrishnan and V. Balakrishnan, J. Low Temp. Phys. **5**, 81 (1971).
- ²⁰C. Ebner and C. C. Sung, Phys. Rev. A **4**, 269 (1971); Phys. Rev. A **4**, 1099 (1971).
- ²¹W. M. Fairbank and G. K. Walters, *Proceedings of the Symposium on Liquid and Solid Helium Three* (Ohio State Research Foundation, Columbus, Ohio, 1957), p. 220.
- ²²E. D. Adams, H. Meyer, and W. M. Fairbank, *Helium Three*, edited by J. G. Daunt (Ohio State U. P., Columbus, Ohio, 1960), p. 57.
- ²³H. A. Reich, Phys. Rev. **129**, 630 (1963).
- ²⁴R. L. Garwin and A. Landesman, Phys. Rev. **133**, A1503 (1964).
- ²⁵A. L. Thomson, H. Meyer, and P. N. Dheer, Phys. Rev. **132**, 1455 (1963).
- ²⁶R. C. Richardson, E. Hunt, and H. Meyer, Phys. Rev. **138**, A1326 (1965).
- ²⁷R. C. Richardson, A. Landesman, E. Hunt, and H. Meyer, Phys. Rev. **146**, 244 (1966).
- ²⁸M. G. Richards, J. Hatton, and R. P. Giffard, Phys. Rev. **139**, A91 (1965).
- ²⁹R. P. Giffard and J. Hatton, Phys. Rev. Lett. **18**, 1106 (1967).
- ³⁰W. Senghaphan and G. O. Zimmerman, Phys. Rev. Lett. **20**, 371 (1968); *Proceedings of the Eleventh International Conference on Low-Temperature Physics*, edited by J. F. Allan, D. M. Finlayson, and D. M. McCall (University of St. Andrews, St. Andrews, Scotland, 1968), p. 344.
- ³¹M. F. Pancyzk, R. A. Scribner, G. C. Straty, and E. D. Adams, Phys. Rev. **19**, 1102 (1967); M. F. Pancyzk and E. D. Adams, Phys. Rev. **187**, 321 (1969); R. A. Scribner, M. F. Pancyzk, and E. D. Adams, J. Low Temp. Phys. **1**, 313 (1969).
- ³²H. D. Cohen, P. B. Pipes, K. L. Verosub, and W. M. Fairbank, Phys. Rev. Lett. **21**, 677 (1968).
- ³³M. G. Richards and J. M. Homer, Phys. Rev. **182**, 318 (1969).
- ³⁴J. M. Homer and M. G. Richards, Phys. Rev. Lett. **22**, 273 (1969).
- ³⁵R. T. Johnson, R. Rosenbaum, O. G. Symko, and J. C. Wheatley, Phys. Rev. Lett. **22**, 449 (1969); R. T. Johnson, O. G. Symko, and J. C. Wheatley, Phys. Rev. Lett. **23**, 1017 (1969).
- ³⁶A. C. Anderson, G. L. Salinger, W. A. Steyert, and J. C. Wheatley, Phys. Rev. Lett. **7**, 295 (1961).
- ³⁷P. B. Pipes and W. M. Fairbank, Phys. Rev. Lett. **23**, 520 (1969); Phys. Rev. A **4**, 1590 (1971).
- ³⁸J. R. Sites, D. D. Osheroff, R. C. Richardson, and D. M. Lee, Phys. Rev. Lett. **23**, 836 (1969).
- ³⁹W. P. Kirk, E. B. Osgood, and M. Garber, Phys. Rev. Lett. **23**, 833 (1969).
- ⁴⁰W. N. Yu and H. A. Reich, Solid State Commun. **7**, 1521 (1969).
- ⁴¹P. N. Henriksen, M. F. Pancyzk, and E. D. Adams, Solid State Commun. **8**, 735 (1970).
- ⁴²A. C. Anderson, W. Reese, and J. C. Wheatley, Phys. Rev. Lett. **7**, 366 (1961); R. T. Johnson and J. C. Wheatley, Phys. Rev. A **1**, 1836 (1970).
- ⁴³D. S. Miyoshi, R. M. Cotts, A. S. Greenberg, and R. C. Richardson, Phys. Rev. A **2**, 670 (1970).
- ⁴⁴M. Bernier, J. Low Temp. Phys. **3**, 29 (1970).
- ⁴⁵M. Bernier and A. Landesman, Solid State Commun. **7**, 529 (1969).
- ⁴⁶A. Landesman and M. Bernier, Solid State Commun. **8**, 2151 (1970).
- ⁴⁷E. B. Osgood and M. Garber, Phys. Rev. Lett. **26**, 353 (1971).
- ⁴⁸W. P. Kirk and E. D. Adams, Phys. Rev. Lett. **27**, 392 (1971).
- ⁴⁹The assumption that the sum in Eq. (1) need include only nearest-neighbor interactions has recently been questioned (Refs. 16 and 30).
- ⁵⁰The distinction between pure He³ and mixtures with small concentrations of He⁴ is clearly artificial. The purest samples used to date contained about a part in 10⁷ He⁴. We use the distinction only to separate those investigations into the properties of solid He³ from those into the effect produced by adding He⁴ impurity.
- ⁵¹R. A. Guyer, R. C. Richardson, and L. I. Zane, Rev. Mod. Phys. **43**, 532 (1971).
- ⁵²M. G. Richards, *Advances in Magnetic Resonance*, edited by J. S. Waugh (Academic New York, 1971).
- ⁵³G. A. Baker, H. E. Gilbert, J. Eve, and G. S. Rushbrook, Phys. Rev. **164**, 800 (1967).
- ⁵⁴R. C. Richardson, J. Phys. (Paris) Suppl. **31**, C3-79 (1970).
- ⁵⁵Cryocal, Inc., Riviera Beach, Fla. and Scientific Instruments, Lake Worth, Fla.
- ⁵⁶Five other GRT's from Scientific Instruments were tested and none behaved satisfactorily. The most probable cause of this unsatisfactory behavior was lead breakage upon temperature cycling.
- ⁵⁷Gollob Analytical Service Corporation, Berkeley Heights, N.J.
- ⁵⁸T. R. Roberts, R. H. Sherman, and S. G. Sydorik, J. Res. Natl. Bur. Stand. (U.S.) A **68**, 567 (1964).
- ⁵⁹Vapor pressure thermometry was not used below 0.8 K because of the controversy on the exact nature of the thermomolecular corrections [cf. G. T. McConville, Cryogenics **9**, 122 (1969)]. The two vapor pressure tubes were included in our apparatus to enable us to attempt to measure the correction *in situ* by the differential method suggested by Watkins and co-workers [R. A. Watkins, W. L. Taylor, and W. J. Hanbach, J. Chem. Phys. **46**, 1007 (1967)]. This method proved unreliable to within the accuracy we required.
- ⁶⁰W. G. Clark, Rev. Sci. Instrum. **35**, 316 (1964).
- ⁶¹C. R. Bruce, R. E. Norberg, and G. E. Pake, Phys. Rev. **104**, 419 (1956).
- ⁶²The equivalent parallel circuit is obtained by replacing the actual tank circuit consisting of a coil with inductance L_0 and resistance R , in parallel with a capacitor C , by an almost equivalent circuit with R' , C , and L_0 all in parallel, where $R' = L^2 \omega^2 / R$. This procedure is only valid for high- Q circuits and low signal measurements (i.e., if L does not change significantly during the sample resonance).

⁶³Extraction of χ from a measure of the area under the resonance line, as is sometimes done, is not feasible for very high accuracy measurements such as those reported here. The usual analysis connecting the area and χ is not necessarily valid for the case of He³, where practical running conditions give line shapes that deviate significantly from Lorentzian, and contain large contributions of free precession signal (see Sec. II D). In addition, most spectrometers will have nonlinearities amounting to at least a percent or so over the range of resonance-line voltage detected, and these nonlinearities would be difficult to account for in measuring the area under the line.

⁶⁴B. A. Jacobsohn and R. K. Wangsness, *Phys. Rev.* **73**, 942 (1948).

⁶⁵M. R. Gabillard, *C.R. Soc. Biol. (Paris)* **232**, 96 (1951).

⁶⁶That T_2 may have a small temperature dependence poses no problem, since $I''(t')$ is found to be only very weakly dependent upon T_2 . Calculation showed that for a change of T_2 from 30 to 250 msec (the range of T_2 's for our samples) $I''(t')$ changed only about 5%. The height of the experimental

resonance line where $\chi' = 0$, when corrected for changes in filling factor, was also observed to change only 5% over this range of T_2 's. Since T_2 is known to be constant to about $\pm 5\%$ or better in the data-collecting temperature regions of our experiments (Refs. 24 and 27), changes in T_2 could only give spurious line-height changes of less than 0.04%.

⁶⁷K. A. Kermach and J. B. S. Haldane, *Biometrika* **37**, 30 (1950).

⁶⁸E. R. Grilly and R. L. Mills, *Ann. Phys. (N.Y.)* **8**, 1 (1959); R. L. Mills, E. R. Grilly, and S. G. Sydorak, *Ann. Phys. (N.Y.)* **12**, 41 (1961).

⁶⁹W. J. Mullin, *Phys. Rev. Lett.* **20**, 254 (1968).

⁷⁰T. P. Bernat, Ph.D. thesis (Brandeis University, 1972) (unpublished).

⁷¹Y. Beers, *Introduction to the Theory of Error* (Addison-Wesley, Reading, Mass., 1957).

⁷²P. R. Benington, *Data Reduction and Error Analysis for the Physical Sciences* (McGraw-Hill, New York, 1969).

Solid-Solid and Solid-Fluid Phase Transitions in Terms of the Lattice Model

Tsuyoshi Horiguchi and Tomoyasu Tanaka*

Department of Physics, Ohio University, Athens, Ohio 45701

(Received 31 August 1972)

The order-disorder theory of a classical lattice model is used to obtain both the solid-solid phase transition and fluid-solid phase transition in a single system. In this model, the range of the interatomic potential is extended up to the fourth-neighbor distance. If the potential is suitably chosen, it is shown that the phase transitions between the bcc solid and fcc solid, between the bcc solid and fluid, and between the fcc solid and fluid occur within the Bragg-Williams approximation. The results are shown by the phase diagrams.

I. INTRODUCTION

Since Lennard-Jones and Devonshire¹ (LJD) formulated a theory of melting of solids in terms of the lattice model, the lattice model has been used by many authors in order to investigate theoretically the phase transition between the solid and fluid.^{2,3} A satisfactory explanation at least in the first approximation, has been given for the change of phase from the solid to the fluid in terms of the interatomic forces.

Recently, LJD theory has been refined and extended by Yoshida and Okamoto⁴ to explain the melting curve maximum, which is a fascinating phenomenon found at high pressures. (This must be distinguished from the critical temperature for the coexistence of solid and liquid. The melting curve maximum implies that it is not possible to transform solid phase continuously into liquid phase, in contrast with the case between liquid phase and gas phase.) In their theory, like in LJD theory, the ratio of the number of occupied lattice points to that of unoccupied lattice points is fixed and hence the volume change of the system is represented by the change in the lattice constant. By using an ef-

fective interatomic potential, the repulsive part of which is properly soft, and using the Bragg-Williams approximation, they obtained a melting curve which has a maximum in T - P phase diagram.

In high-pressure experiments,⁵⁻¹⁰ not only the melting curve maximum but also solid-solid phase transitions have been observed in several substances. It is now a well-established fact that some substances, e.g., Ce, Cs, and so on, undergo polymorphic transitions which contain several structural and also isostructural transitions. In some cases of isostructural transition, the mechanism is known to be the electronic transition, that is, the promotion of electrons from one shell to another or the collapse of one electron shell to another. The mechanism of some structural transitions is known to be the rearrangement of atoms from one structure to another. This may be due partly to the change in the mechanism of cohesion resulting from the electronic transition, but mostly to statistical effects. The typical example of the structural and isostructural transition is observed in the phase diagram of cesium,^{6,8} which is shown in Fig. 1. The two separate experimental results are superposed in one figure. The experi-